ELSEVIER

Journal of Fluids and Structures 21 (2005) 321–333

JOURNAL OF FLUIDS AND STRUCTURES

www.elsevier.com/locate/jfs

Characteristics of the turbulent boundary layer pressure spectra for high-speed vessels

E. Ciappi*, F. Magionesi

INSEAN- Istituto Nazionale per Studi ed Esperienze di Architettura Navale, Via di Valleranno 139, 00128 Rome, Italy

Received 27 September 2004; accepted 15 July 2005
Available online 10 October 2005

Abstract

Recent studies demonstrate that the fluctuating pressure field generated by the turbulent boundary layer (TBL) is an important flow noise source for high-speed marine vehicles. In fact, wall-pressure fluctuations induce vibrations in the hull plates of the vessel that are responsible for undesirable noise on board. In this framework, the correct description of the pressure load acting on the hull needs a deep knowledge of its spectral features and, in this work, the problem of the power spectral density characterization is analysed. This quantity is usually obtained experimentally, because of limitations of the available computational resources at the high Reynolds numbers typical of engineering applications. However, the experimental evaluation of the power spectral density presents as well some problems because of the low frequency pollution due to the background noise of the facilities and because of the high frequency attenuation due to the finite size of the pressure sensors. Boundary-layer characteristics depend, for a body moving in an unbounded flow, on the Reynolds number, while, in the case of a surface ship, a Froude number dependency must be taken into account. In view of the evaluation of the noise level on board of civil high-speed vessels generated by flow-induced vibrations, an experimental campaign aimed at measuring the pressure fluctuations beneath the TBL attached to the hull of a ship model was performed in a towing tank. The use of this facility, new for this kind of experiments, provides ideal flow conditions because background noise and turbulence are absent. Pressure signals are acquired for a large range of Reynolds numbers by varying both the model velocity and the test-section along the hull length. With this experimental set-up it was possible to analyse the details of the pressure spectra in the different frequency regions. In this work, a detailed discussion on the pressure scaling laws is provided together with a critical comparison with the available results obtained for different facilities and experimental conditions.

Keywords: Wall pressure fluctuations; Scaling laws; High speed vehicles

1. Introduction

The characterization of wall-pressure fluctuations beneath turbulent boundary layers (TBLs) has received the attention of the scientific community since the early '60s (Corcos, 1963, 1964; Willmarth and Wooldridge, 1962) due to the great number of engineering problems related to this phenomenon. The most popular of them are related to fatigue damage of aircraft fuselages, noise radiation in the aircraft cabin, and the sonar-masking phenomenon in marine

*Corresponding author. Tel.: +39 06 50299268; fax: +39 06 5070619.
E-mail address: e.ciappi@insean.it (E. Ciappi).

0889-9746/$ - see front matter © 2005 Elsevier Ltd. All rights reserved.
doi:10.1016/j.jfluidstructs.2005.07.006

military applications. However, wall-pressure fluctuations are also important in the mechanism of noise radiation from piping systems and, recently, due to the development of new concept designs for high-speed vessels, in civil marine applications. In fact, an increase in ship speed gives rise to an increase of noise level on board, mainly due to the propulsion system, to the on-board engines and to the hydrodynamic noise sources including breaking waves, propeller cavitation and the TBL on the ship hull. Recent studies performed in the framework of the European RTD project Noise Reduction for Marine Applications (NORMA) showed that hull vibrations excited by the TBL must be carefully considered in the evaluation of the total noise level on board. In this paper some of the results, achieved during this project, on the wall-pressure experimental analysis are presented.

The main difference between the work available in the technical literature on this subject and the current study is the presence of a free surface flow. Besides a Reynolds number ($\mathrm{Re} = UL/v$) dependency, the free surface introduces a Froude number ($\mathrm{Fr} = U/\sqrt{gL}$) dependency of the TBL, where U is the free-stream velocity, in this case the ship speed, L is a reference length, g the gravity acceleration, and v the kinematic viscosity. It is clear that, even considering calm water conditions, the waves generated by the ship itself during navigation can be at least responsible for local pressure gradients causing acceleration or deceleration of the flow that affect the boundary layer. However, if the boundary-layer characteristics are evaluated far from the free water surface where three-dimensional effects are important, the Froude dependency is taken into account by the velocity parameters, and the problem can be considered equivalent to that of an unbounded flow with pressure gradients. The aim of this work is to provide a description of the wall-pressure spectra, measured on a model of a high speed trimaran, with particular attention to the scaling laws of the power spectral density (PSD). As was extensively discussed by Bull (1967), wall pressure fluctuations receive contributions from velocity fluctuations in all parts of the boundary layer. Moreover, since it is well known that there is not a unique law to scale the velocity field and that turbulent structures at various distances from the wall are convected at different velocities, it is not possible to find an unique representation of the PSD in the whole frequency range. On the other hand, the determination of the correct scaling laws for the pressure spectra provides information about the contributions of the different TBL regions on the wall-pressure spectra. Moreover, with reference to the present application, the possibility of representing with universal curves the different PSD frequency regions can provide a chance for the estimation of the full-scale pressure spectra starting from pressure measurements on the model. In fact, as will be clear when discussing the scaling parameters, the nondimensional pressure spectra can be rescaled by using the boundary layer mean velocity parameters of the full size problem that can be easily computed by relatively low time consuming RANSE numerical simulations.

However, the frequency characterization of the PSD is very complicated because, at low frequency, it is very difficult to separate the boundary-layer contribution from the background noise of the facility and, at high frequency, the finite size of the pressure sensors is responsible for attenuation in the spectra.

The problem was analysed experimentally and theoretically by several authors (Bull, 1967; Bradshaw, 1967; Panton and Linebarger, 1974; Blake, 1986; Farabee and Casarella, 1991; Keith et al., 1992; Gravante et al., 1998) and numerically by Choi and Moin (1990) and Chang et al. (1999). The PSD frequency range is subdivided into different frequency regions that correspond to different scaling laws and, for this analysis, the division proposed by Farabee and Casarella (1991) is used. Farabee and Casarella (1991) identified four frequency ranges in their data: the low frequency and the mid-frequency range where outer variables hold, the high frequency range where inner variables hold, and an overlap scale-independent region proportional to ω^{-1}, ω being the circular frequency, whose extent depends on the Reynolds number.

For the sake of clarity in what follows, δ indicates the boundary layer thickness, δ^* and ϑ the displacement and the momentum thickness, respectively, and ρ the fluid density. Moreover u_τ is the friction velocity, τ_w the shear stress, $\phi(\omega)$ the pressure power spectral density and q the dynamic pressure.

While it is well established that the inner variables $\omega v/u_\tau^2$, $\phi(\omega)u_\tau^2/(\tau_w^2 v)$, provide the appropriate scaling law for the high frequency part of the spectra, different outer scaling are proposed in the literature. With respect to this, Keith et al. (1992) presented the most extensive comparison between many available experimental data obtained in fully developed and developing channel flow, in fully developed pipe flow and in the wind tunnel, over a wide range of Reynolds numbers, with the aim of identifying the best choice for the scaling parameters in the different frequency regions. The numerical results by Choi and Moin (1990) were also considered. The results of their analysis showed that, for the mid-frequency range, the outer variables that used the dynamic pressure as pressure scale and δ^*/U as time scale, generating the nondimensional quantities $\omega\delta^*/U$ and $\phi(\omega)U/(4q^2\delta^*)$, provide in general the best collapse of the data. However, when considering data measured at low Reynolds numbers, i.e. for $\mathrm{Re}_\vartheta = U\vartheta/v < 4500$, the variables $\omega\delta^*/U, \phi(\omega)U/(\tau_w^2\delta^*)$, obtained by introducing the shear stress as pressure scale seemed to be the best choice to obtain a collapse of data at mid-frequencies. Finally, in the high frequency range, the validity of the inner variables was confirmed, even if the comparison between different measurements performed with different sizes of sensors is questionable for a large part of the frequency range. Since the low frequency range is not covered by most of the

experiments, it was not discussed in the Keith et al. paper. In a previous study, Farabee and Casarella (1991) assessed different conclusions on the basis of wind tunnel measurements performed with small pressure sensors. Using noise cancellation techniques, they were able to show the behaviour of the pressure spectrum at very low frequency, where an ω^2 dependence is outlined, confirming the Lilley and Hodgson and Ffowcs Williams predictions [see Ffowcs Williams (1982)]. In this frequency range the validity of the outer variables, obtained by using the dynamic pressure, is stated. On the contrary they found that in the mid-frequency region the data collapse when the outer scaling $\omega\delta/u_\tau, \phi(\omega)u_\tau/(\tau_w^2\delta)$, proposed by Panton and Linebarger (1974), is used. Finally, by direct inspection of the range of validity of the outer and the inner scaling, they identified an overlap region between the mid- and the high frequency range, even if the characteristic ω^{-1} slope is not clearly displayed, because the *Re* values are just above the minimum value suggested by Panton and Linebarger (1974), i.e. $\mathrm{Re}_\tau = u_\tau\delta/\nu > 333$.

The characterization of the low frequency spectral behaviour, although containing less than 1% of the total energy, could be important for applications, because the typical resonance or coincidence frequencies of many structures can lie in this range. The theoretically predicted ω^2 behaviour of the spectra is considered valid, even if the experimental evidence was obtained only in a few cases. Facility and instrumentation noise, vibrations and, in the case of free-field experiments, pressure gradients can alter this trend. In fact, contradictory conclusions were assessed in glider data: Hogdson found in at first the ω^2 fall-off with decreasing frequency and in later measurements a flat trend; while Panton et al. (1980) found a weak fall-off of the spectra. The existence of an overlap region between the mid- and the high frequency ranges was predicted for the first time by Bradshaw (1967) on the basis of some unpublished experimental data and by dimensional analysis. Bradshaw predict an $\omega^{-0.8}$ behaviour and demonstrated that this region is associated with pressure sources in the logarithmic part of the boundary layer. Panton and Linebarger (1974) showed that if an overlap region exists, it should exhibit an ω^{-1} behaviour, and its extension is dependent on the Reynolds number. Concerning the effects of the finite size of the pressure sensors, Willmarth and Roos (1965) and Schewe (1983) examined the influence on pressure spectra of different pressure sensors and of different sensor size, while Corcos (1963) proposed a correction formula of the measured spectra, based on his cross-spectral density model, that is the theoretical method still used for high frequency data correction. Finally, a detailed review of the state of the art can be found in Bull (1996). It is clear from the above references that, especially for engineering applications, the problem is always analysed experimentally, because the numerical solution of the Poisson equation governing the pressure field in a turbulent flow is impossible to achieve at high Reynolds numbers with the available computational resources. Some numerical results can be found in the cited Choi and Moin (1990) work where the channel flow problem is analysed for $\mathrm{Re}_\vartheta = 287$ and in Chang et al. (1999) that analysed the influence of the different TBL velocity components on the wavenumber pressure spectra in a channel flow and for $\mathrm{Re} = 3200$.

The present data, acquired for a large Reynolds number range, i.e. for $4500 < \mathrm{Re}_\vartheta < 14\,200$, obtained by varying both the free-stream velocity and the test-section and in a low noise facility, give a detailed description of the PSD behaviour and of its scaling laws in the whole frequency range. Comparison with the results of other authors demonstrates the validity of the results obtained.

2. Experimental facility and set-up

The experiments took place in the INSEAN towing tank N.1. This hydrodynamic facility is 480 m long, 12 m wide, 6 m deep and it is provided with a carriage. The carriage drive system is an electric one with 4-pairs of drive wheels, each pair provided with a main motor. The maximum carriage speed is 15 m/s with accuracy better than $\pm 0.1\%$.

The use of a towing tank is particularly challenging for this kind of experiments: in fact, flow conditions can be considered ideal, because problems related to free-stream disturbances or to the presence of background turbulence and noise, as in wind or water tunnels, are avoided.

The experimental tests were performed in calm water on a 1:35 model of the trimaran SES MISTRAL, designed by Alstom Chantiers de l'Atlantique (see Fig. 1). The scale of the model was chosen, as usual, according to the Froude similarity law, being impossible to respect Re similarity. Three test-sections (in what follows indicated as bow, middle and stern section respectively), located on the trimaran's V-shaped central hull (see Fig. 2) were provided. The coordinates x_s along the keel, y_s in the transverse direction, and z_s in the vertical direction of the sensors' position, measured with respect to a reference system with origin on the bow bottom and on the keel line of the central hull, are listed in Table 1. The calm water line with respect to the same reference system is located at $z_s = 0.05$ m, and the distance between the central and the external hulls, measured on the water line, is 0.26 m. This last information, compared with the actual δ values reported in Table 2, ensures that the boundary layers attached to the three hulls were not influenced by each other. The angle between the central hull edges and the water plane is constant for each

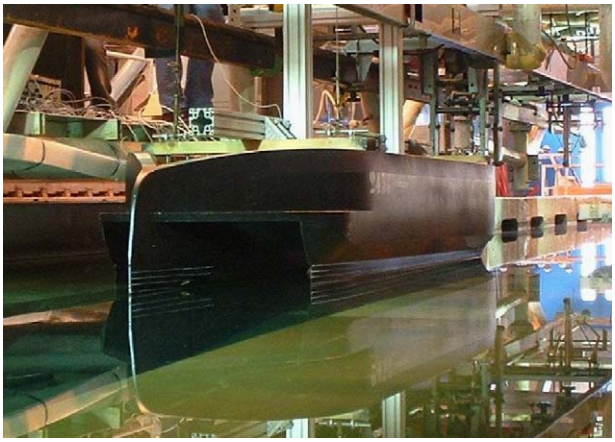

Fig. 1. Trimaran model.

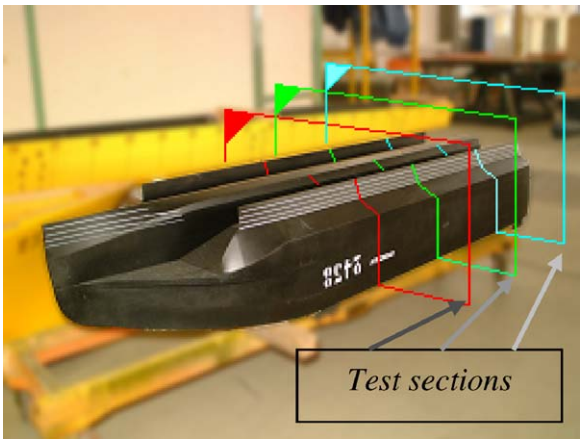

Fig. 2. Test-section locations.

Table 1
Model principal dimensions and location of measuring sections

Maximum length (m)	3.142
Maximum width (m)	0.91
x_{s1}, y_{s1}, z_{s1}(m)	1.447, 0.042, 0.0063
x_{s2}, y_{s2}, z_{s2} (m)	2.137, 0.042, 0.0056
x_{s3}, y_{s3}, z_{s3} (m)	2.715, 0.042, 0.0049

transverse section and, in correspondence to the test-sections, varies along the keel between 9° in the stern part and 11° in the bow part. A schematic view of the hull geometry and of the sensor positions with respect to the water line is shown in Fig. 3.

In this way the test conditions can be varied by varying both the model velocity, thus varying Reynolds and Froude numbers at the same time, and the measuring section; in this last case the Froude number remains constant. In each section, a plexiglas window, 1 cm thick, was inserted for positioning the transducers, and the windows were attached with some mastic in order to attenuate the transmitted carriage vibrations.

Nevertheless, structural vibration peaks, mostly due to the interaction between the rails and the wheels of the carriage and transmitted through the rigid connections between the carriage and the model necessary to maintain the ship trim, were present in the pressure spectra. Model vibrations were, in this case, particularly severe, because of the small draft

Table 2
Boundary layer velocity parameters

U (m/s)	Fr	δ (m)	δ^* (m)	θ (m)	Re_ϑ	u_τ (m/s)	$d_0 = d/\delta^*$	$d^+ = du_\tau/\nu$
Bow section								
2.6	0.46	2×10^{-2}	3.05×10^{-3}	2.26×10^{-3}	4.53×10^3	0.11	0.1–0.32	25–84
3.47	0.62	2.06×10^{-2}	3.03×10^{-3}	2.34×10^{-3}	6.25×10^3	0.1421	0.1–0.33	33–109
4.34	0.78	2.04×10^{-2}	2.97×10^{-3}	2.3×10^{-3}	7.68×10^3	0.1761	0.11–0.34	40–135
5.2	0.93	1.96×10^{-2}	2.83×10^{-3}	2.19×10^{-3}	8.78×10^3	0.2086	0.11–0.35	48–160
Middle section								
2.6	0.46	2.68×10^{-2}	3.93×10^{-3}	2.84×10^{-3}	5.68×10^3	0.106	0.07–0.25	24–81
3.47	0.62	2.73×10^{-2}	3.9×10^{-3}	2.92×10^{-3}	7.79×10^3	0.1378	0.07–0.25	32–106
4.34	0.78	2.73×10^{-2}	3.84×10^{-3}	2.89×10^{-3}	9.66×10^3	0.1695	0.08–0.26	39–130
5.2	0.93	2.71×10^{-2}	3.75×10^{-3}	2.85×10^{-3}	1.14×10^4	0.182	0.08–0.26	48–160
Stern section								
2.6	0.46	3.32×10^{-2}	4.75×10^{-3}	3.46×10^{-3}	6.93×10^3	0.103	0.06–0.21	24–79
3.47	0.62	3.39×10^{-2}	4.73×10^{-3}	3.58×10^{-3}	9.54×10^3	0.1347	0.06–0.21	31–103
4.34	0.78	3.3×10^{-2}	4.53×10^{-3}	3.45×10^{-3}	1.15×10^4	0.1655	0.07–0.22	38–127
5.2	0.93	3.45×10^{-2}	4.65×10^{-3}	3.55×10^{-2}	1.42×10^4	0.194	0.06–0.21	44–149

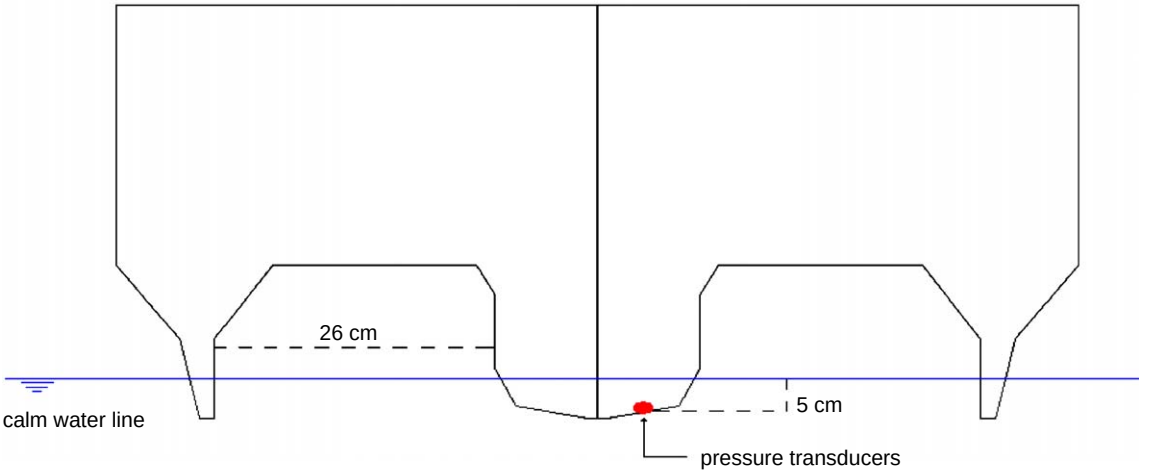

Fig. 3. Schematic view of the central hull section.

of the vessel that reduces the damping water action. However, such disturbances are limited to a few discrete spectral lines and do not mask the trends in the pressure spectra. This is a great advantage with respect to wind or water tunnels where the disturbances are superimposed to the pressure spectra over a large continuous frequency range.

Pressure measurements were performed with differential piezoresistive pressure transducers Endevco 8510-B, characterized by a maximum range of 2 psig and by a certified flat response until 14 kHz. The transducers were calibrated in air. The deviation around the regression line of the data points, used for the sensitivity estimate, was evaluated. The standard error of estimate was very low for all the transducers, of the order of 1%. The use of a static calibration in air can introduce a bias error when the transducers are used in water. For this reason a static calibration in water using a known water level height was performed for some transducers. Also, in this case the transducers showed a linear trend but revealed small sensitivity variations, with respect to the case in air, of about 2%. Finally the total error due to thermal sensitivity, nonlinearity and pressure hysteresis was around 1%. The rectangular sensing element had an area, not declared in the data sheet but deduced by a direct inspection of the transducers by removing the external protection grid, of $1 \times 0.3\,\mathrm{mm}^2$. Usually the pressure sensors used for similar analyses have a circular cross-section and, to estimate the effect of the spatial attenuation due to their finite size, it is assumed that their sensitivity is constant over the surface and two different nondimensional parameters were defined. The first, based on the outer

characteristic length δ^*, is $d_0 = d/\delta^*$, and the second, based on the viscous length ν/u_τ is $d^+ = du_\tau/\nu$, where d is the sensor diameter. It is clear that in the present case the exact definition of these parameters is not trivial. If, on the other hand, the streamwise dimension is considered as suggested by Corcos (1963) and as adopted by Keith et al. (1992) to compare the numerical Choi and Moin data, only a range of variation for d_0 and d^+ can be assessed, because the position of the sensing element with respect the mean flow velocity direction is unknown, being hidden by the protection grid. Obviously, d_0 and d^+ strongly depend on the Reynolds number; thus, their values, for each velocity and for each test-section, are reported in Table 2 when $d = 0.3$ mm and when $d = 1$ mm. Looking at the d_0 and d^+ values obtained, it is clear that, even considering the worst cases, these pressure sensors ensure a quite good description of the pressure spectra, being in line with many of those used to obtain the most significant experimental results available [see Keith et al. (1992)]. The comparison of the $p_{r.m.s}$ values and of the high-frequency decays in the spectra obtained in the present and in other authors' experiments can give an estimation of the real d_0 and d^+ values.

Pressure signals were acquired and amplified by the 16-channel acquisition system PROSIG; the sampling frequency was 8 kHz. In the bow section, eight transducers are flush-mounted on the hull in order to analyse also their spatial behaviour (not reported here), while in the middle and in the stern sections a single transducer was provided. Additional pressure transducers located far from the previous ones were used to remove from the spectra the vibration peaks.

Flow velocity components are, in a first phase, measured by means of two-component back-scatter laser Doppler velocimetry (LDV), from the internal part of the model through the plexiglas windows. Unfortunately, the relatively big dimensions of the LDV measuring volume with respect to the actual TBL thickness did not allow the resolution with good accuracy of the logarithmic region for all the test conditions and, thus, the velocity data were obtained by numerical simulations. The numerical code description is provided in the next section.

Pressure signals were acquired for four different ship model velocities, 2.6, 3.47, 4.34 and 5.2 m/s, and several repetitions of the tests (typically 12–15) under nominally the same conditions were performed.

3. Velocity field analysis

The velocity field around the whole trimaran model was obtained by solving the Reynolds-averaged Navier–Stokes equations (RANSE) that describe the turbulent motion of an incompressible (constant density) viscous fluid.

In the present work, the turbulent viscosity was calculated by means of the Spalart and Allmaras (1994) one-equation model. The problem is closed by enforcing appropriate conditions at physical and computational boundaries. On solid walls, the velocity is set to zero (whereas no condition on the pressure is required); at the (fictitious) inflow boundary, the velocity is set to the undisturbed flow value, and the pressure is extrapolated from inside; on the contrary, the pressure is set to zero at the outflow, whereas the velocity is extrapolated from inner points.

The major difficulty in solving the RANSE lies in the solenoidal constraint on the velocity vector field. When only the average steady state must be computed, the divergence-free constrain can be conveniently substituted by an evolution equation for the pressure [see Chorin (1967)]. By doing so, the system of equations is hyperbolic in its Eulerian part; therefore, all the numerical methods developed for the compressible flow simulation can be adapted and applied to the above system.

The RANSE are approximated by a finite volume technique, with pressure and velocity co-located at the cell centre; the algorithm is identical to the one described in Di Mascio et al. (2001) and will be only briefly recalled here; the reader is referred to the cited paper for details.

The residual on each control volume is computed as a flux balance at the cell interfaces. In order to obtain second-order accuracy in space, the stress tensor has to be evaluated at the centre of the cell interfaces. To this end, the velocity gradients are computed by means of a standard second-order centred finite volume approximation on a volume made of the two half-cell volumes adjacent to each interface. For the inviscid part, a second-order Essentially NonOscillatory (ENO) scheme (Harten et al., 1987) was adopted, i.e. convective fluxes are computed as the solution of a Riemann problem at the cell interface, whose left and right state are obtained by a second-order extrapolation from the closest cell centres. In order to simplify the algorithm, a second-order accurate solution of the Riemann problem [see Di Mascio et al. (2001)] is used in place of the exact one (which should be computed iteratively, given the nonlinearity of the problem). It can be shown that the resulting scheme is second-order accurate, and yields oscillation-free discrete solutions, also when the exact solutions are discontinuous. Time integration of the discrete model is achieved by means of a standard implicit scheme with approximate factorization (Beam and Warming, 1978). The convergence to steady-state is accelerated by local time stepping and a multi-grid algorithm [for more details and the performance of this technique applied to time marching ENO schemes, see Favini et al. (1996)]. Finally, a Level Set technique was used to capture the free surface.

The principal boundary layer characteristics including all the parameters necessary for the pressure scale, obtained from the analysis of the longitudinal velocity profiles, are reported in Table 2. The errors of the numerical simulations affect obviously the computation of TBL parameters, determining an uncertainty of about 4% in their estimation.

The results of the numerical simulations proved that the boundary layer on the central hull was in fully developed conditions in all the test-sections and that the ship wave pattern did not exhibit breaking wave phenomena. However, the wave field affects the boundary layer characteristics, inducing local acceleration or deceleration of the flow, depending on the considered ship velocity. The order of magnitude of the induced pressure gradients can be given by the parameter $\Pi = (\nu/\rho U^3)(\mathrm{d}p/\mathrm{d}x)$, its maximum value was estimated equal to 0.5.

4. Pressure results

The pressure signals were analysed in the frequency domain determining their auto spectral density using 400 ensemble sets containing 4096 data. Thus, the statistical convergence error $\varepsilon_r = 1/\sqrt{n_d}$, where n_d is the number of ensemble sets, is about 5%. The uncertainty in the calculated pressure spectra, obtained by considering all the previously defined sources of error, is within the range of ± 1 db.

As outlined before, high peaks in the frequency region between 9 and 13 Hz due to structural vibrations of the carriage were present. The peaks were eliminated using suitable relations based on the coherence function (Bendat and Piersol, 1991) between two pressure sensors located, for each test-section, on the plexiglas windows but sufficiently far apart to be correlated only with the structural vibrations. The result of this cleaning procedure is shown in Fig. 4.

Let us know discuss the validity of the spectra scaling laws for the present data. In Fig. 5 the spectra obtained by the measured pressure signals in the middle section, by varying the ship velocity, scaled with the outer variables defined using q, are shown. It is evident that there is a good collapse of the data for $0.06 < \omega\delta^*/U < 1.8$. Following Blake (1986), attenuation in the spectra occurs for $\omega d/U > 1.2$ that implies $\omega\delta^*/U > 4.5$ or $\omega\nu/u_\tau^2 > 0.18$ when considering $d = 1$ mm and the boundary layer parameters relative to 5.2 m/s in the present data. The scaled spectra exhibit a maximum for $0.2 < \omega\delta^*/U < 0.25$, confirming the results of Farabee and Casarella (1991) expressed as $\omega\delta/u_\tau = 50$. Moreover, for $\omega\delta^*/U < 0.1$, a fall-off of the curves appears, confirming the trend found by several investigators. Unfortunately it is not possible to understand if the ω^2 trend is kept. In fact, although the data clearly show a decreasing trend at very low frequencies, the exact behaviour cannot be unequivocally detected by comparing all measurements for different velocities and for different sections. This fact can be due to local flow disturbances, probably located in the bow part of the model, or to the presence of slightly different pressure gradient values. For this reason we chose to cut the spectra below 8 Hz.

In the same figure a comparison with the results of different authors, not corrected for spatial resolution errors, extracted from Keith et al. (1992), is provided. It can be noted that the present data, characterized by $5680 < \mathrm{Re}_\vartheta < 11\,400$ fall between the Farabee data for $\mathrm{Re}_\vartheta = 3400$ and the Bull data for $\mathrm{Re}_\vartheta = 19\,500$; they also seem to be in a good agreement with the Bull and Thomas results for $\mathrm{Re}_\vartheta = 7000$. An increasing trend of the spectra with decreasing Reynolds number is in accordance with many experimental results [see Keith et al. (1992)]. In Fig. 6 the same spectra are plotted using the outer scaling proposed by Farabee and Casarella (1991). It is evident again that an excellent collapse of the data for $10 < \omega\delta/u_\tau < 300$ is obtained, that roughly corresponds to the same frequency range of Fig. 5. The data, in this case, are compared with the Farabee and Casarella (1991) results obtained for $\mathrm{Re}_\vartheta = 6050$ but coincident, in the mid-frequency range, with the results for $\mathrm{Re}_\vartheta = 3386$ and $\mathrm{Re}_\vartheta = 4487$ and with the results of Gravante et al. (1998) obtained for $\mathrm{Re}_\vartheta = 4548$. It is evident that an excellent agreement is obtained for $10 < \omega\delta/u_\tau < 200$. Unfortunately it is not possible to make comparisons with the same data in the two different scales and to find in the technical literature data for very high Reynolds numbers scaled with the Farabeee and Casarella outer scaling. Since the same spectral behaviour displayed in Figs. 5 and 6 was observed for all the cases examined, i.e. for all the possible combinations of test-sections and velocities, some conclusions can be reached. The fact that using the dynamic pressure and the free-stream velocity as scaling parameters produces a dispersion of the data can be considered an effect of the Reynolds number. On the other hand, the use of the shear stress and the friction velocity seems to reduce this scatter, at least when low Reynolds number data are included in the comparison; thus, it represents the best choice to provide data collapse in the mid-frequency range. However, the evidence that the actual data, measured for quite a large range of Reynolds numbers, scale with both scaling laws suggests that, in comparing different data sets, a deep examination of the experimental conditions and of the experimental errors must be included to provide general conclusions. The best way to proceed should be a wide Reynolds number range analysis on the basis of experimental data acquired using the same experimental set-up.

In Fig. 7 the previous spectra, scaled with the inner variables, are shown. A collapse occurs only for $0.05 < \omega\nu/u_\tau^2 < 0.13$ because, for higher nondimensional frequencies, the finite size of the pressure sensors caused

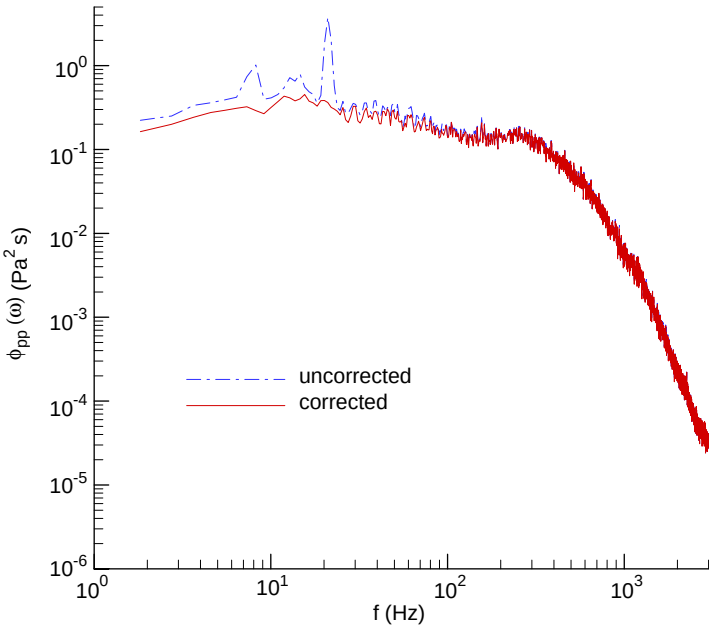

Fig. 4. Measured and cleaned pressure spectral density.

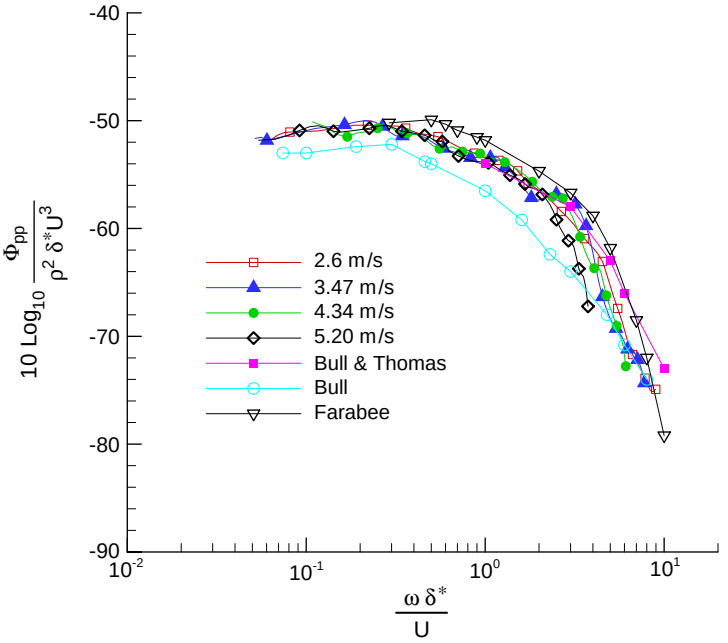

Fig. 5. Power spectral densities in the middle section scaled with the outer variables $\omega\delta^*/U$, $\phi_{pp}/\rho^2\delta^* U^3$.

attenuation in the spectra. However, from the analysis of Figs. 5–7 it is evident that both the outer and the inner variables hold for a region between the mid-and the high frequencies, i.e. in the overlap region where the ω^{-1} dependency is evident (see Fig. 6). As was outlined by Panton and Linebarger (1974) and by Farabee and Casarella (1991), the overlap region appears only for $\mathrm{Re}_\tau = u_\tau\delta/\nu > 333$ and its extension depends on the Reynolds number. The Re_τ values for the data shown in Figs. 5–7 varied from 2185 to 4148, and the extent of the region expressed in outer

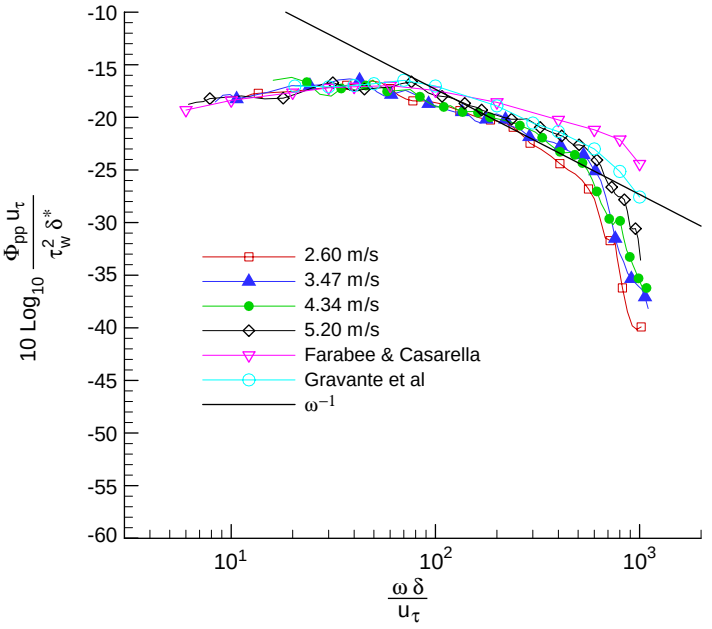

Fig. 6. Power spectral densities in the middle section scaled with the outer variables $\omega\delta/u_\tau$, $\phi_{pp}u_\tau/\tau_w^2\delta$.

variables is $0.65<\omega\delta^*/U<1.8$ or $130<\omega\delta/u_\tau<300$. In Fig. 7 the comparison with the data of previous investigators shows that all of them collapse in the overlap region but exhibit completely different trends for higher frequencies. It can be concluded that, for d_0 and d^+ values characterizing the plotted spectra, no information about the high frequency region can be extracted. To better clarify this point, let us analyse the spectra measured for the same velocity but in the three different sections. In Fig. 8 the spectra measured for 2.6 m/s, scaled with the inner variables, are shown. In this case, Re_ϑ as well as the d_0 and d^+ values are the smallest of the whole data set (see Table 2), and sensor resolution errors appear for $\omega\nu/>u_\tau^2 0.3$. From the analysis of Fig. 8 it is evident that a good data collapse is obtained for $0.08<\omega\nu/u_\tau^2<0.3$ and that the overlap region is not visible because the Re_τ values lie close to the minimum value suggested. The extent of the overlap region, obtained by direct inspection of the mid and high frequency scaling-law validity, expressed in outer variables, is $1<\omega\delta^*/U<1.8$, while in terms of inner variables it is $0.08<\omega\nu/u_\tau^2<0.13$. Thus, for $\omega\nu/u_\tau^2>0.13$, the high frequency region appears. The comparison with the data of Farabee and Casarella ($d^+=0.33$) and of Bull and Thomas ($d^+=0.44$) shows a better agreement with respect to the data plotted in Fig. 7, but a quite large difference in the spectral amplitude, for $\omega\nu/u_\tau^2>0.1$, is still visible. Notwithstanding this, the trend of the present spectra seems to be in good agreement with the $\omega^{-7/3}$ behaviour, typical of this frequency region [see Farabee and Casarella (1991)].

In Figs. 9 and 10 the spectra obtained for 3.47 and 4.34 m/s, scaled with the inner variables, are shown. By the inspection of these figures it is clear that, so long as the Reynolds number increases, the extension of the overlap region increases. Comparing the inner variables of Figs. 9 and 10 with the outer variables (not reported here) for the same velocities, it appears that the upper value of the overlap region is always $\omega\nu/u_\tau^2=0.13$, while its lower value is $\omega\nu/u_\tau^2=130/\mathrm{Re}_\tau$, confirming the results displayed in Figs. 5–7. Finally, it is important to stress that for 4.34 m/s (see Fig. 10) there is an excellent agreement with Bull's curve, obtained with $d^+=170$, against $d^+=130$ estimated from the present data, indicating that the values of Table 2 are reliable.

The last observation regards the Froude number dependency of the pressure spectra. As was stated before, the presence of the free surface is responsible for local acceleration or deceleration of the flow and, as a consequence, for pressure gradients. Panton and Linebarger (1974) showed that pressure gradients cause an increase of the spectrum level in the outer law and mid-frequency range while its effect tends to zero when approaching the high frequencies. However, in the present case, pressure gradients are extremely small, namely $\Pi=0.5$ or in an equivalent way $k=(\nu/\rho U^3)(\mathrm{d}p/\mathrm{d}x)=3\times10^{-6}$; hence, their effect on the pressure spectra is negligible. The evidence that the spectra presented exhibit a good collapse with data obtained for ideal flow conditions demonstrates that pressure gradients can be considered negligible. As discussed above, their effect can play a role only in the very low frequency region.

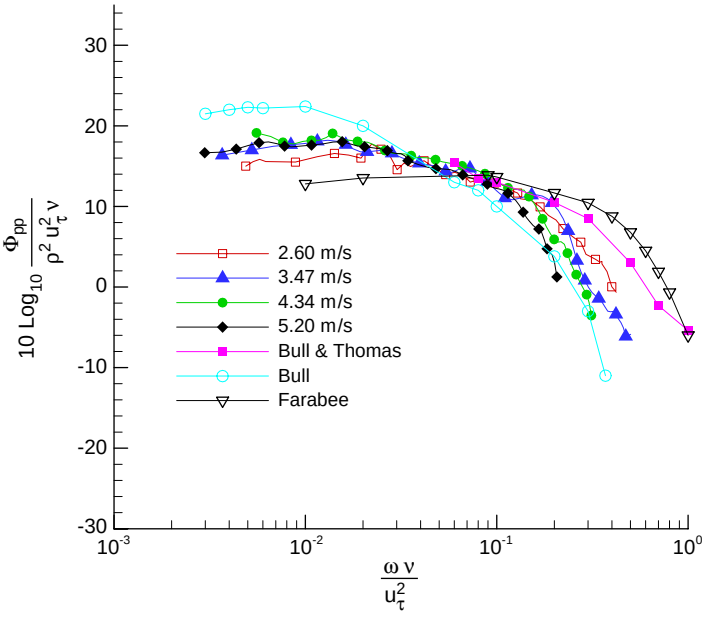

Fig. 7. Power spectral densities in the middle section scaled with the inner variables $\omega\nu/u_\tau^2$, $\phi_{pp}/\rho^2 u_\tau^2 \nu$.

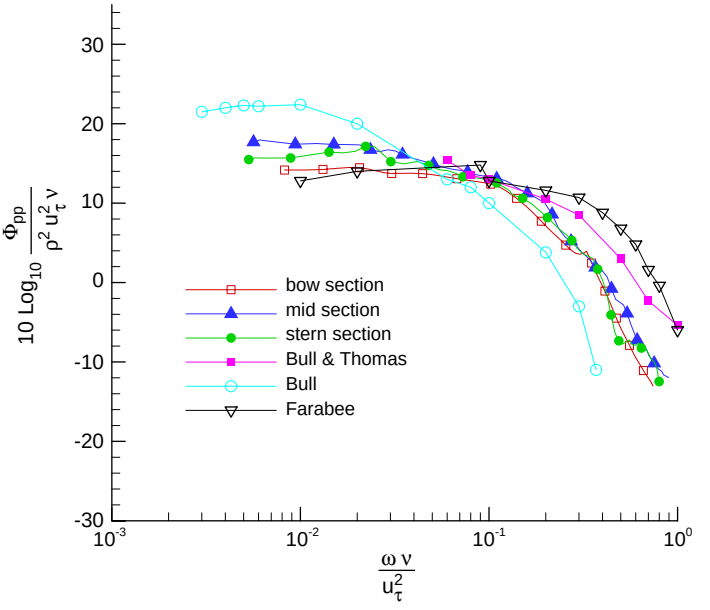

Fig. 8. Power spectral densities for 2.6 m/s scaled with the inner variables $\omega\nu/u_\tau^2$, $\phi_{pp}/\rho^2 u_\tau^2 \nu$.

From the above considerations it can be concluded that: (i) the present data scale with both the outer variables proposed for $0.06 < \omega\delta^*/U < 1.8$ or $10 < \omega\delta/u_\tau < 300$; (ii) an overlap region exists for all the test conditions in the range $130/\mathrm{Re}_\tau < \omega\nu/u_\tau^2 < 0.13$; and (iii) the inner variables hold for $\omega\nu/u_\tau^2 > 0.13$.

Finally, the root-mean-square of the pressure fluctuations was obtained by integrating the cleaned power spectral density. This quantity is very sensitive to experimental disturbances and, in general, its values present a large scatter for different test conditions, mainly because of the different high frequency resolution due to the finite sensors size. In Fig. 11 the obtained nondimensional p_{rms} values together with some of the data reported in Farabee and Casarella (1991) are plotted as a function of $\mathrm{Re}_\tau = u_\tau\delta/\nu$. In the same figure the theoretical curve obtained by Farabee and

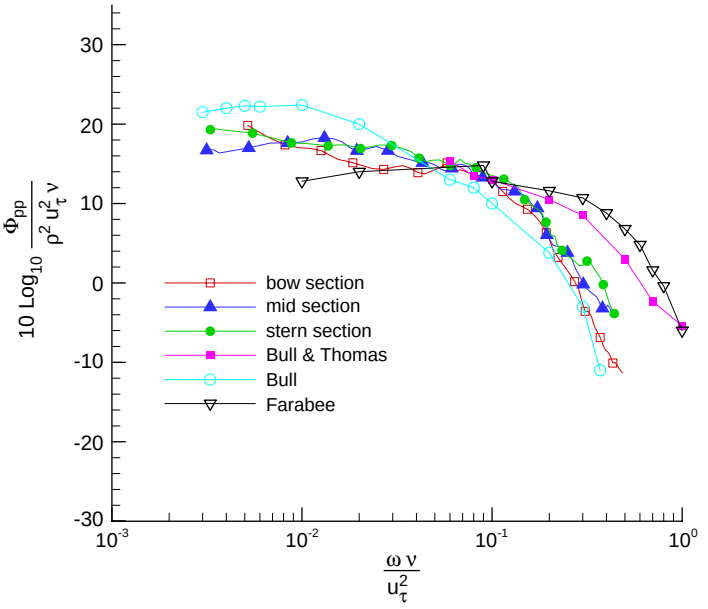

Fig. 9. Power spectral densities for 3.47 m/s scaled with the inner variables $\omega\nu/u_\tau^2$, $\phi_{pp}/\rho^2 u_\tau^2 \nu$.

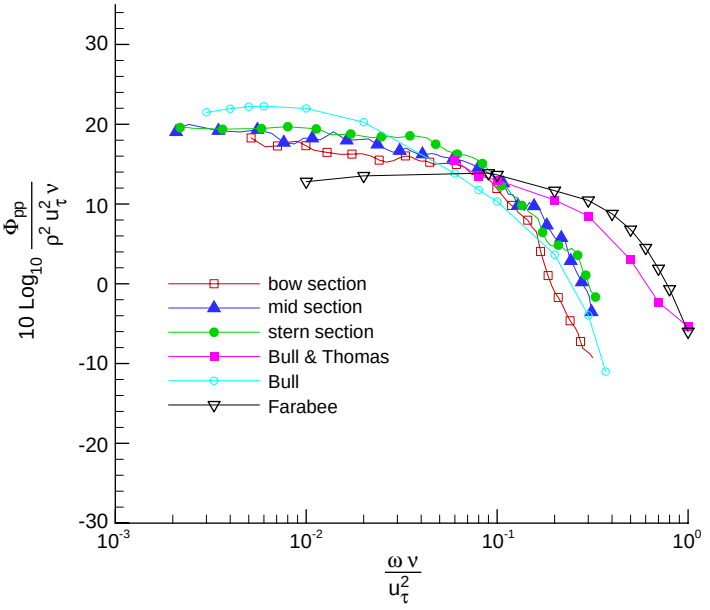

Fig. 10. Power spectral densities for 4.34 m/s scaled with the inner variables $\omega\nu/u_\tau^2$, $\phi_{pp}/\rho^2 u_\tau^2 \nu$.

Casarella,

$$\frac{p_{\text{r.m.s}}^2}{\tau_w} = \begin{cases} 6.5, & \text{Re}_\tau < 333 \\ 6.5 + 1.86 \ln\left(\frac{\text{Re}_\tau}{333}\right), & \text{Re}_\tau > 333 \end{cases}$$

is also displayed. This equation was obtained by integrating their experimental spectrum for $5 < \omega\delta/u_\tau < 100$, thus excluding the low-frequency part, and integrating the spectrum over the overlap region ($100 < \omega\delta/u_\tau < 0.3\text{Re}_\tau$) assuming that it follows the ω^{-1} law. Finally the high-frequency contribution was obtained using the Bull high-frequency empirical formula to avoid transducer resolution error.

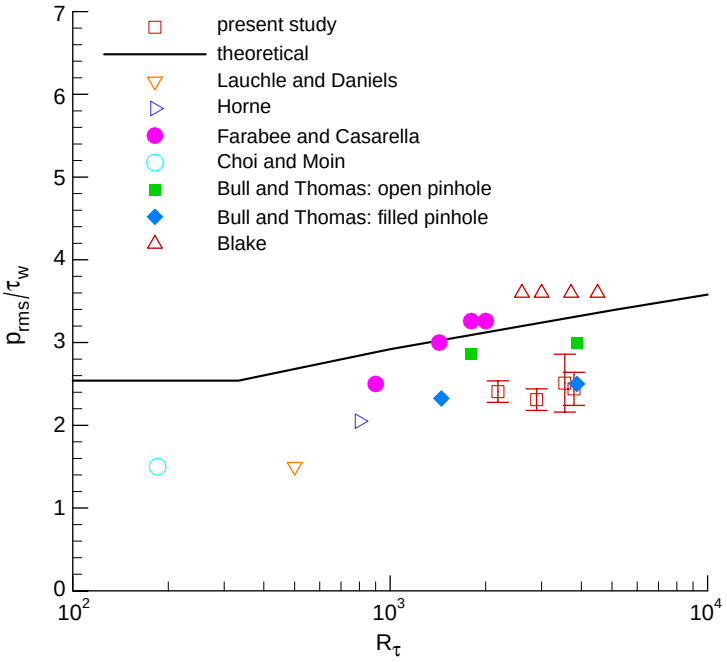

Fig. 11. Nondimensional root-mean-square of pressure fluctuations.

The error bars on the present data represent the uncertainty for a 95% confidence level using a Student-t distribution based on three independent measurements. From the analysis of the figure it is evident that $p_{\mathrm{r.m.s}}/\tau_{\mathrm{w}}$ values are Reynolds-number dependent, thus complicating the comparison between different data sets. The present results, relative to the middle test-section and to the four different velocities, but comparable with the one obtained in the other sections for similar Re_τ, exhibit lower values with respect to the Farabee and Casarella, Blake and Bull and Thomas data, all obtained with an open pinhole microphone. This fact can be explained with the different high frequency behaviour of the spectra (see Figs. 7–10). However, the $p_{\mathrm{r.m.s}}$ values are comparable with those of Bull and Thomas (1976), obtained by filled pinhole microphones and with piezoelectric transducers that, as reported by Bull (1996), gave a better pressure estimation with respect to the open pinhole microphone when considering the same d^+ value.

5. Conclusions

In this work the results of an experimental programme performed in a towing tank and devoted to wall-pressure fluctuation measurements on a model of a high-speed vessel are discussed. Although pressure spectra depend on the Froude number, it is shown that, for the present problem, the pressure scaling laws do not change, because the pressure gradients generated by the waves are negligible. It is shown that, with the analysis performed by varying both the test-section and the velocity, a quite accurate description of the pressure spectra in the low, mid-, overlap and high frequency regions is possible. The most appropriate inner and outer scaling laws for these regions are provided as well as their ranges of validity. The results obtained are compared, when possible, with some of the most significant experimental data available, obtained in different facilities and under different test conditions, and with the theoretical laws describing the spectral behaviour in the different frequency ranges, showing a very good agreement.

Acknowledgements

The authors wish to thank Dr Andrea Di Mascio for the numerical analysis of the velocity field and for many helpful suggestions.

This research was supported by the E.U. in the frame of the RTD NORMA (Noise Reduction for Marine Applications) project G3RD-2001-0393.

References

Beam, R.M., Warming, R.F., 1978. An implicit factored scheme for the compressible Navier–Stokes equations. AIAA Journal 16, 393–402.

Bendat, J.S., Piersol, A.G., 1991. Random Data: Analysis and Measurements Procedure. Wiley & Sons, New York.

Blake, W.K., 1986. Mechanics of Flow Induced Sound and Vibration. Academic Press, Orlando.

Bradshaw, P., 1967. 'Inactive' motion and pressure fluctuations in turbulent boundary layers. Journal of Fluid Mechanics 30, 241–258.

Bull, K.M., 1967. Wall pressure fluctuations associated with subsonic turbulent boundary layer flow. Journal of Fluid Mechanics 28, 719–754.

Bull, M.K., 1996. Wall pressure fluctuations beneath turbulent boundary layers: some reflections on forty years of research. Journal of Sound and Vibrations 190, 299–315.

Bull, M.K., Thomas, S.W., 1976. High frequency wall pressure fluctuations in turbulent boundary layers. Physics of Fluids 19, 597–599.

Chang, P.A., Piomelli, U., Blake, W.K., 1999. Relationship between wall pressure and velocity-field sources. Physics of Fluids A 11, 3434–3448.

Choi, H., Moin, P., 1990. On the space-time characteristics of wall pressure fluctuations. Physics of Fluids A 2, 1450–1460.

Chorin, A., 1967. A numerical method for solving incompressible viscous flow problems. Journal of Computational Physics 2, 12–26.

Corcos, G.M., 1963. Resolution of pressure in turbulence. Journal of the Acoustical Society of America 35, 192–199.

Corcos, G.M., 1964. The structure of turbulent pressure field in boundary-layer flows. Journal of Fluid Mechanics 18, 353–377.

Di Mascio, A., Broglia, R., Favini, B., 2001. A second order Godunov-type scheme for naval hydrodynamics. In: Toro, E.F. (Ed.), Godunov Methods: Theory and Applications. Kluwer Academic/Plenum Publishers, New York, pp. 253–261.

Farabee, T.M., Casarella, M.J., 1991. Spectral features of wall pressure fluctuations beneath turbulent boundary layers. Physics of Fluids A 3, 2410–2420.

Favini, B., Broglia, R., Di Mascio, A., 1996. Multi-grid acceleration of second order ENO schemes from low subsonic to high supersonic flows. International Journal of Numerical Methods in Fluids 23, 589–606.

Ffowcs Williams, J.E., 1982. Boundary layer pressures and the Corcos model: a development to incorporate low wavenumber constraints. Journal of Fluid Mechanics 125, 9–25.

Gravante, S.P., Naguib, A.M., Wark, C.E., Nagib, H.M., 1998. Characterisation of the pressure fluctuations under a fully developed turbulent boundary layer. AIAA Journal 36, 1811–1816.

Harten, A., Engquist, B., Osher, S., Chakraverthy, S.R., 1987. Uniformly high order accurate essentially non-oscillatory schemes. Journal of Computational Physics 71, 231–303.

Keith, W.L., Hurdis, D.A., Abraham, B.M., 1992. A comparison of turbulent boundary layer wall-pressure spectra. ASME Journal of Fluids Engineering 114, 338–347.

Panton, R.L., Linebarger, J.H., 1974. Wall pressure calculations for equilibrium boundary layers. Journal of Fluid Mechanics 65, 261–287.

Panton, R.L., Goldman, A.L., Lowery, R.L., Reischman, M.M., 1980. Low-frequency pressure fluctuations in axisymmetric turbulent boundary layers. Journal of Fluid Mechanics 97, 299–319.

Schewe, G., 1983. On the structure and resolution of wall-pressure fluctuations associated with turbulent boundary-layer flow. Journal of Fluid Mechanics 134, 311–328.

Spalart, P.R., Allmaras, S.R., 1994. A one-equation turbulence model for aerodynamic flows. La Recherche Aérospatiale 1, 5–21.

Willmarth, W.W., Roos, F.W., 1965. Resolution and structure of the wall pressure field beneath a turbulent boundary layer. Journal of Fluid Mechanics 22, 81–94.

Willmarth, W.W., Wooldridge, C.E., 1962. Measurements of the fluctuating pressure at the wall beneath a thick turbulent boundary layer. Journal of Fluid Mechanics 14, 187–210.